Batteries & Supercaps

Research Article
doi.org/10.1002/batt.202200215

Chemistry Europe
European Chemical Societies Publishing

www.batteries-supercaps.org

Free-Standing Pearl-Chains-like MoO_2 Hierarchical Nanowires with Enhanced Pseudocapacitive Energy Storage

Changwei Shi,[a] Shihao Feng,[a] Xinyuan Li,[a] Jianyong Zhang,[a] and Liqiang Mai*[a, b]

Nanostructure construction is an efficient strategy to achieve high pseudocapacitive behavior with excellent charge storing ability and good cyclability. In this work, we constructed a novel pearl-chains-like MoO_2 nanowires (MoO_2 PNWs) on nickel foam via a facile solvothermal method. The formation mechanism can be inferred from the oriented growth and self-assembly process under the contribution of benzyl alcohol and sodium dodecyl sulfate (SDS). The MoO_2 PNWs deliver a high specific capacitance of 1254 $F g^{-1}$ at 1 $A g^{-1}$, outstanding rate performance with 73% retention from 1 to 20 $A g^{-1}$, and 91.5% retention of capacitance after 2000 cycles at 10 $A g^{-1}$. The outstanding performance is attributed to the continuous electron conductive path, short ion diffusion length and enlarged electrode-electrolyte interface provided by the pearl chains like hierarchical nanowire, and good electrical conductivity owing to the free-standing structures.

Introduction

In the context of increasing energy demand and serious environmental pollution, the investigation and utilization of green and renewable energy are significant.[1–3] Due to the intermittency of clean energy sources, such as wind energy and solar energy, realizing high-efficiency energy storage is very important for utilizing green electricity.[4–6] Supercapacitors (SCs), which bridge the gap between batteries and electrostatic capacitors, have received numerous research interests owing to their fast charge-discharge rate, high power density, and long cyclability.[7–9] Among various types of SCs, pseudocapacitors (PCs) possess higher charge storing ability compared to electric double-layer capacitors (EDLCs), in which electrical energy is mainly stored through a reversible Faradaic reaction.[10–13]

Various materials have been explored as active electrode materials for pseudocapacitors, including metal salts, transition metal oxides, conducting polymers, and hydroxides.[14–19] Among them, MoO_2 is an up-and-coming candidate attributed to its low electrical resistance, the different oxidation states of Mo, and natural abundance.[20–23] Take Mo (IV)/Mo (VI) as a redox reaction pair, the theoretical capacitance is as high as 2512.6 $F g^{-1}$ at the voltage windows of 0.6 V. However, bulk MoO_2-based PCs still face challenges with low rate ability and inferior cyclability, which are limited by the sluggish charge transportation, restricted accessible active sites, and poor structural durability.[24–26]

To achieve desirable charge storage properties, various strategies have been devoted to boost the electron transport rate and ion diffusion kinetics of electrode materials.[27,28] Constructing pseudocapacitors electrode materials with different sizes and nano architectures, such as one-dimensional (1D) nanowires and hollow structures, has been demonstrated to be an effective way to improve electrochemical activity.[29–32] Among them, 1D nanowires can provide 1D continuous conduction paths and short ion diffusion lengths, facilitating ion diffusion into the bulk of the electrode.[33–35] In addition, hierarchical nanostructures have the benefits of a large specific surface area, more accommodating active sites and enlarged electrode-electrolyte interface, thereby enhancing the rate capability.[36] Another effective approach is preparing free-standing electrodes through direct growth nanowires on conductive substrates, such as nickel foam, which increases the electrical conductivity.[37,38] Inspired by the above, the rational design and synthesis of free-standing 1D hierarchical MoO_2 nanowires for high pseudocapacitive storage are highly desirable. However, the construction of nanostructured MoO_2 still has challenges, including rationally controlling the nucleation and growth processes and efficiently reducing Mo(VI) precursors to low-valent Mo(IV) oxides. Hydrogen reduction or thermal decomposition has been reported to synthesize MoO_2, but its nanostructures are difficult to tune rationally.[39–42] To date, the nanostructure design of MoO_2 for supercapacitors are mainly reported in nanoparticles,[43–45] nanorods,[20,27,46] nanospheres,[47,48] the 1D hierarchical nanowires are rarely reported.[49,50] Therefore, it is essential to choose suitable reducing agents and surfactants to explore the synthesis of 1D MoO_2 hierarchical nanowires under mild conditions.

[a] C. W. Shi, S. H. Feng, X. Y. Li, J. Y. Zhang, Prof. L. Q. Mai
State Key Laboratory of Advanced Technology for Materials Synthesis and Processing
Wuhan University of Technology
Wuhan 430070, P. R. China
E-mail: mlq518@whut.edu.cn
[b] Prof. L. Q. Mai
Foshan Xianhu Laboratory of the Advanced Energy Science and Technology Guangdong Laboratory
Xianhu hydrogen Valley, Foshan 528200, P. R. China

Supporting information for this article is available on the WWW under https://doi.org/10.1002/batt.202200215

An invited contribution to a Special Collection dedicated to the 5-Year Anniversary of Batteries & Supercaps

Research Article
doi.org/10.1002/batt.202200215
Chemistry Europe
European Chemical Societies Publishing

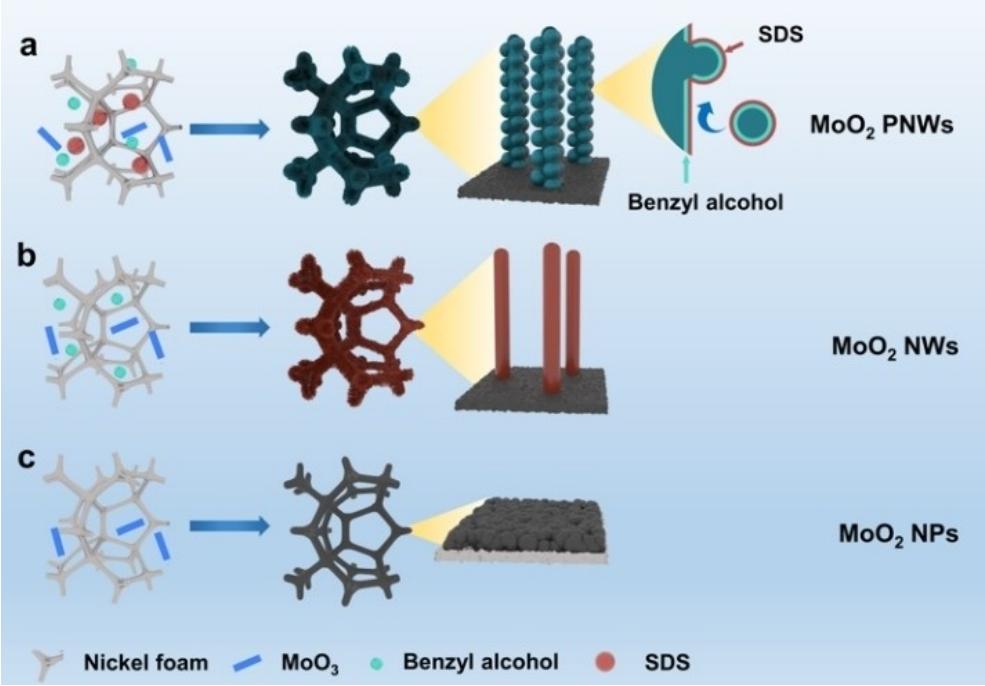

Figure 1. Schematic illustration for the synthesis of MoO_2 PNWs, MoO_2 NWs, and MoO_2 NPs.

Herein, we fabricated a free-standing MoO_2 pearl-chains-like nanowires (MoO_2 PNWs) grown on the nickel foam through a solvothermal method, significantly improving pseudocapacitive energy storage. The formation mechanism can be inferred from the oriented growth and self-assembly process under the action of benzyl alcohol and sodium dodecyl sulfate (SDS). The MoO_2 PNWs grown on nickel foam display a pearl-chains-like structure consisting of vertical nanowires as chains and nanoparticles as pearls, and possess advantages as follows: (1) the 1D nanowires provide continuous electron conductive path and short ion diffusion length; (2) the hierarchical nanostructures expose more accommodating active sites and enlarge the electrode-electrolyte interface; (3) the free-standing structures increase the electrical conductivity. When tested in 2 M KOH solution, the MoO_2 PNWs deliver a high specific capacitance of 1254 $F g^{-1}$ at 1 $A g^{-1}$, and 91.5% retention of capacitance after 2000 cycles at 10 $A g^{-1}$. Our work developed an effective synthesis strategy to architecture 1D MoO_2 hierarchical nanowires and demonstrated the promising application for pseudocapacitive energy storage.

Results and Discussion

As schematically illustrated in Figure 1a, we synthesized free-standing MoO_2 PNWs grown on the nickel foam through a facile solvothermal method. Firstly, the MoO_3 nanobelts were synthesized through a typical approach.[41] Then, the as-prepared MoO_3 powder, benzyl alcohol, and SDS were dispersed well in a methanol/water solution. After that, nickel foam and the above solution were put into autoclaves and treated under 180 °C for 48 hours. After washing and drying, the MoO_2 PNWs grown on the nickel foam were obtained. For comparison, the bare MoO_2 nanowires without hierarchical structure (MoO_2 NWs) grown on nickel foam were prepared without the reactant of SDS (Figure 1b). While the MoO_2 nanoparticles (MoO_2 NPs) grown on the nickel foam were prepared by a similar process without benzyl alcohol and SDS reactants (Figure 1c).

The scanning electron microscopy (SEM) image depicts that the MoO_2 PNWs are vertically and uniformly grown on the nickel foam substrate (Figure 2a). The MoO_2 PNWs present a pearl-chains-like structure consisting of vertical nanowire as a chain and nanoparticles as pearls (Figure 2b). The overall diameter of MoO_2 PNWs is around 200 nm, and the length

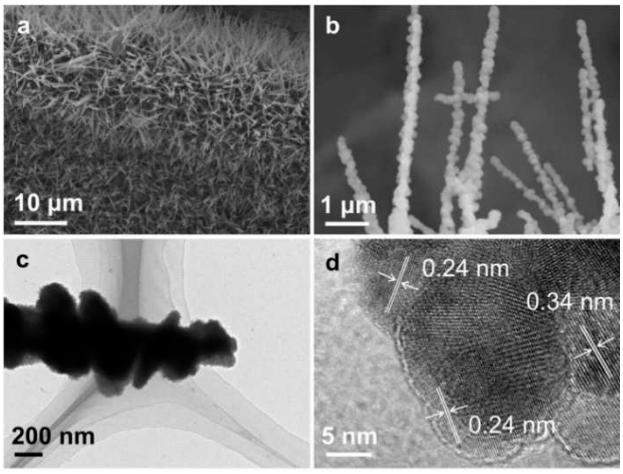

Figure 2. a, b) SEM images, c) TEM image, d) HRTEM image of MoO_2 PNWs.

ranges from 5–10 μm. The transmission electron microscopy (TEM) image depicts the rough surface of attached nanoparticles (Figure 2c), suggesting more active sites during redox reactions. A high-resolution TEM (HRTEM) image indicates the nanoparticles are well crystallized, the lattice spacings were measured to be 0.34 nm and 0.24 nm, matching well with the (111) plane and (−111) plane of MoO_2 (Figure 2d). In addition, the surface area was investigated by N_2 sorption. The specific surface area of MoO_2 PNWs reaches as high as 141.4 $m^2 g^{-1}$ according to the Brunauer-Emmett-Teller (BET) result, which is larger than that of MoO_2 NWs (95.9 $m^2 g^{-1}$) and MoO_2 NPs (39.8 $m^2 g^{-1}$) (Figure S5).

To investigate the growth mechanism, controlled experiments were conducted to determine the function of benzyl alcohol and SDS. When no SDS was added during the synthesis, the prepared MoO_2 could not generate the pearl-chains-like hierarchical structure, indicating that SDS affects the self-assembly process (Figure S1). It can therefore be speculated that nanoparticles are assembled on the nanowire surface by directional attachment due to the presence of SDS, the intrinsic driving force of which is the reduction of Gibbs energy during the SDS coating layer and crystal surface.[44,45] As the addition amount of benzyl alcohol was reduced, 1D nanowire structures were no longer generated, revealing that benzyl alcohol plays a crucial role in promoting the directional growth of MoO_2 nanowires, possibly due to adsorption-mediated reduction and crystal growth (Figure S2). When there is no addition of both benzyl alcohol and SDS, the as-prepared MoO_2 NPs show nanoparticle structure without generation of nanowires and hierarchical structure (Figure S3). Time-dependent experiments on MoO_2 NPWs were also performed to observe the growth process of MoO_2 PNWs (Figure S4). Based on the above results, we propose the formation mechanisms of MoO_2 PNWs into two continuous and simultaneous stages: oriented growth and self-assembly. Specifically, MoO_3 dissolves in solution to form $Mo_2O_7^{2-}$ and MoO_4^{2-} (minority species) anions. These anions are then reduced to MoO_2 by benzyl alcohol and methanol. A proportion of MoO_2 nucleates on the substrate forming isolated islands, while the rest becomes precipitates. With the continuous supply of MoO_2, the islands grow into interconnected networks and thin film (Figure S4a). Subsequently, the nanowires grow vertically from the film through oriented growth (Figure S4b). Finally, pearl chains like nanowires were generated through a self-assembly process (Figure S4c). During the formation process, benzyl alcohol and SDS play important role in achieving free-standing MoO_2 1D hierarchical nanowires.

The X-ray diffraction (XRD) pattern of MoO_2 PNWs shows diffraction peaks at 26.0°, 37.1°, 53.5°, 60.5°, and 66.2° (Figure 3a), corresponding to the MoO_2 (JCPDS 01-076-1807). XRD patterns of MoO_2 NPs and MoO_2 NWs indicate that they are also composed of the same MoO_2 structures (Figure S6). The surface electronic state of MoO_2 PNWs was investigated through X-ray photoelectron spectroscopy (XPS). The survey spectrum of MoO_2 PNWs depicts peaks of Mo 3d at 233 eV, Mo $3p_{3/2}$ at 398 eV, Mo $3p_{1/2}$ at 415 eV, and O 1s at 531 eV, indicating the presence of Mo and O (Figure 3b). The high-resolution Mo 3d spectrum of MoO_2 PNWs could be deconvoluted into four peaks (Figure 3c). The peaks at 230.5 and

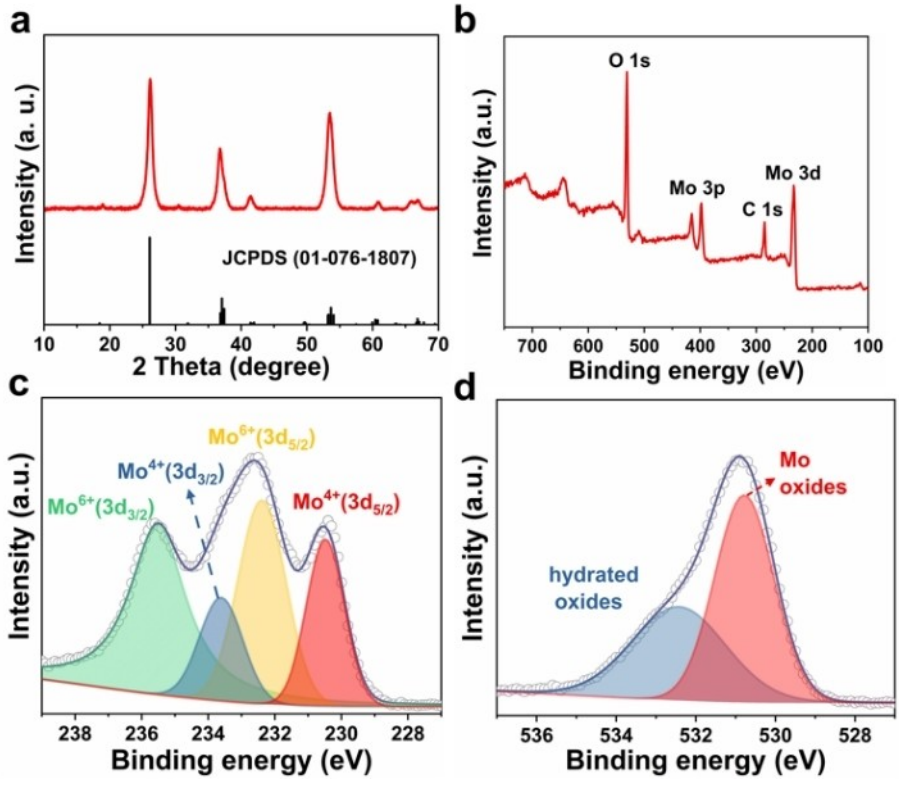

Figure 3. a) XRD pattern; b) XPS survey spectrum; high resolution c) Mo 3d spectrum; d) O 1s spectrum of MoO_2 PNWs.

Research Article
doi.org/10.1002/batt.202200215

233.6 eV can be assigned to the Mo $3d_{5/2}$ and $3d_{3/2}$ of the Mo^{4+} oxidation state.[51,52] The peaks located at 232.4 and 235.5 eV are attributed to Mo $3d_{5/2}$ and $3d_{3/2}$ of the Mo^{6+} oxidation state. The existence of Mo^{6+} is due to the partial oxidation of MoO_2 in air, which is a normal phenomenon for MoO_2.[53,54] The high-resolution O1s spectrum of MoO_2 PNWs is given in Figure 3(d), and it could be deconvoluted into two peaks with the binding energy of 530.8 and 532.4 eV, revealing the presence of two types of oxygen species assigned to molybdenum oxides and surface hydrated oxides, respectively.[55] XPS spectrum of MoO_2 NWs and MoO_2 NPs indicate that they are also composed of a similar surface electronic state (Figure S7).

To evaluate the electrochemical properties of MoO_2 PNWs, cyclic voltammetry (CV) and galvanostatic charge-discharge (GCD) tests were carried out in a 2 M KOH solution using the standard three-electrode system. The CV curves of MoO_2 PNWs are similar in shape and have broad redox peaks at different sweep rates from 2 to 20 $mV\,s^{-1}$ (Figure 4a), suggesting a pseudocapacitive behavior.[56] The symmetric shape and proportional increasing of current density indicate its reversible Faradaic redox properties. As shown in Figure 4b, the MoO_2 PNWs exhibit a high specific capacitance of 1254 $F\,g^{-1}$ at the current density of 1 $A\,g^{-1}$ with an area mass loading of 1.27 $mg\,cm^{-2}$, which is much higher than the reported work (Table S1). Even at the high current density of 20 $A\,g^{-1}$, 925 $F\,g^{-1}$ still be maintained, corresponding to 73% of its maximum capacitance. The performance of MoO_2 NPs and MoO_2 NWs was also tested as a comparison. MoO_2 PNWs demonstrate the best specific capacitance and rate capability among them (Figure 4c).

To study the electrochemical kinetics, the power law of $i = av^b$ was used to analyze the kinetics.[57,58] A quasilinear curve is

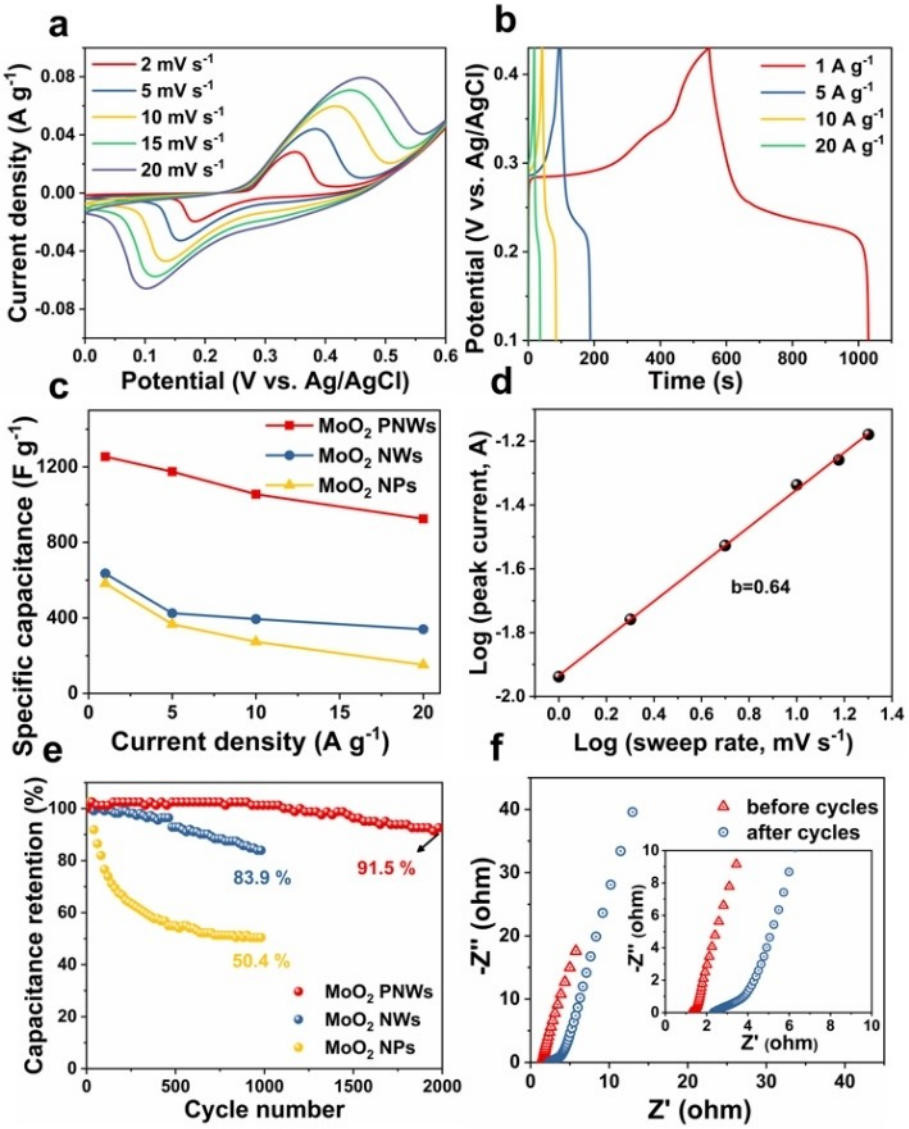

Figure 4. a) CV curves at various sweep rates from 2 to 20 $mV\,s^{-1}$. b) Galvanostatic charge-discharge at the energy density from 1 to 20 $A\,g^{-1}$. c) Rate capability of MoO_2 PNWs, NPs, and NWs from 1 to 20 $A\,g^{-1}$. d) log peak current against log sweep rate for anodic process. e) Cyclability of MoO_2 PNWs, MoO_2 NWs, MoO_2 NPs at 10 $A\,g^{-1}$. (f) Impedance plots of MoO_2 PNWs before and after cycling.

Research Article
doi.org/10.1002/batt.202200215

obtained by plotting the *log i* (peak current) against *log v* (sweep rate) (Figure 4d). According to this law, the b value is calculated by the slope of the linear fit curve. In general, a *b* value of 0.5 suggests diffusion-controlled kinetics, while a *b* value of 1 suggests a surface reaction-controlled behavior. In this work, the b-value is estimated to be 0.64, suggesting the co-existence of both diffusion-controlled and pseudocapacitive type behavior. The as-prepared MoO_2 PNWs exhibit 91.5% retention of specific capacitance after 2000 cycles at the current density of 10 $A g^{-1}$ (Figure 4e), acceptable for pseudocapacitive materials, especially without conductive carbon coating. As a comparison, the MoO_2 NPs and MoO_2 NWs show sluggish cyclability, which may be due to agglomerate and pulverizing for NPs and NWs, respectively. In addition, the electrochemical impedance spectra (EIS) tests were performed before and after 2000 GCD cycles to further investigate the electrochemical cyclability (Figure 4f). The MoO_2 PNWs depict a slight increase of resistance, suggesting good stability during the charge and discharge process.

To investigate the electrochemical storage mechanism, *in-situ* cell was constructed with the as-prepared MoO_2 PNWs as the cathode, active carbon cloth as the anode, and 2 M KOH solution as the electrolyte. Figure S8 depicts the changes in peak intensities and positions of *in-situ* XRD diffraction patterns during three charge/discharge processes of the MoO_2 PNWs electrode. In the 2D patterns shown in Figure S8b, the peak intensities at 36.9° and 53.6° can be observed to drop significantly during discharge and return during charge, indicating that the MoO_2 PNWs undergo a phase transformation process. The 1D patterns in Figure S8(c) show slight lattice expansion/re-contraction, suggesting that the 1D tunnel along an axis and the pearls-like branch provides a fast ion diffusion pathway without destroying the structure of MoO_2 PNWs. Thus, the transition between Mo (IV) and Mo (VI) is proposed to explain the charge storage mechanism.[24,59,60] To study the effects of the electrolyte ion type, the CV tests were carried out in 2 M alkaline electrolyte (LiOH, NaOH, KOH) and 1 M neutral electrolyte (Li_2SO_4, Na_2SO_4, K_2SO_4), respectively (Figure S9). The CV curves in alkaline electrolytes show a much larger enclosed area than in neutral electrolytes, suggesting the main electroactive species are hydroxide. The charge transfer mechanism for this electrochemical process can be expressed as follow: $MoO_2 + 4OH^- \leftrightarrow MoO_4^{2-} + 2H_2O + 2e^-$. During the charge transfer process, OH^- enters the interior space of the bulk through a one-dimensional ion diffusion tunnel, which leads to better utilization of the electrode for higher energy density. Overall, the improved electrochemical performance of MoO_2 PNWs could be derived from the advantages of this pearl chains like nanowire structure: a one-dimensional continuous path for electron transfer and an enlarged surface area to facilitate ion diffusion. Specifically, the inner nanowires provide active sites and conductive pathways for electron transfer, and the outer nanowires enlarge the electrode-electrolyte interface. In addition, it grows directly on a conductive substrate, avoiding the use of binder and improving electronic conductivity.

Conclusion

In summary, we fabricated a free-standing MoO_2 pearl-chains-like nanowires (MoO_2 PNWs) grown on the nickel foam through a facile solvothermal method, which significantly improves pseudocapacitive energy storage. The MoO_2 PNWs grown on nickel foam offer a pearl-chains-like structure consisting of vertical nanowires as chains and nanoparticles as pearls. The formation mechanism can be inferred from the oriented growth and self-assembly process under the contribution of benzyl alcohol and sodium dodecyl sulfate (SDS). The MoO_2 PNWs demonstrates a high energy density of 1254 $F g^{-1}$ at 1 $A g^{-1}$, good rate capability from 1 to 20 $A g^{-1}$ with 73% retention, and 91.5% retention of capacitance after 2000 cycles at 10 $A g^{-1}$. The outstanding performance is attributed to the excellent contact between electroactive materials and substrate, one-dimensional electron conductive pathways provided by nanowire chains, short ion diffusion length, and enlarged electrode-electrolyte interface supplied by the nanoparticle pearls. Our work develops a facile strategy to architecture MoO_2 1D hierarchical nanowires and demonstrates the promising application for pseudocapacitive energy storage.

Experimental Section

All chemicals were purchased from Sinopharm Chemical Reagent Co., Ltd. (Shanghai, China) and used as received without any further purification.

Synthesis of MoO_3: For a typical procedure, 3 g Mo powder was dispersed into 20 mL deionized (DI) water with the ice bath, and 35 mL H_2O_2 was added to the mixture dropwise until the light-yellow solution formed. Stirring for another 2 hours to remove the excessive unreacted H_2O_2, the solution was then transferred into PTFE lined autoclaves for hydrothermal reaction at 180 °C for 12 hours and cooled down to ambient temperature. After centrifugation and washed with DI water, the collected white MoO_3 precursor was dried at 70 °C.

Synthesis of MoO_2 PNWs: 0.1 g as-prepared MoO_3 was grinded and dispersed into 35 mL DI water. After stirring for 20 minutes, 15 mL methanol was added to the above mixture and stirred for 30 minutes. Subsequently, 20 mL benzyl alcohol was added and stirred for another 30 minutes, then 0.3 g sodium dodecyl sulfate (SDS) was added to the above mixture. After stirring for 1 hour, the mixture with a piece of pre-treated nickel foam was transferred into autoclaves and sealed for reaction at 180 °C for 48 hours. After cooling down, the nickel foam was cleaned with DI water and ethanol. After dried in a vacuum at 60 °C, the MoO_2 PNWs grown on nickel foam were obtained.

Synthesis of MoO_2 NWs: MoO_2 NWs were prepared the same way as above, except that no SDS was added to the mixture.

Synthesis of MoO_2 NPs: MoO_2 NPs were prepared the same way as above, except that no SDS and benzyl alcohol were added to the mixture.

Acknowledgements

This work was supported by the National Key Research and Development Program of China (2020YFA0715000), the National Natural Science Foundation of China (51832004, 52127816), and Foshan Xianhu Laboratory of the Advanced Energy Science and Technology Guangdong Laboratory (XHT2020-003).

Conflict of Interest

The authors declare no conflict of interest.

Data Availability Statement

The data that support the findings of this study are available from the corresponding author upon reasonable request.

Keywords: nanowires · MoO_2 · pearl chains like · pseudocapacitive · energy storage

[1] I. Dincer, *Renewable Sustainable Energy Rev.* **2000**, *4*, 157–175.
[2] P. Moriarty, D. Honnery, *Renewable Sustainable Energy Rev.* **2012**, *16*, 244–252.
[3] S. R. Bull, *Proc. IEEE* **2001**, *89*, 1216–1226.
[4] I. H. Rowlands, D. Scott, P. Parker, *Bus. Strat. Env.* **2003**, *12*, 36–48.
[5] R. Ozaki, *Bus. Strat. Env.* **2011**, *20*, 1–17.
[6] A. Hansla, A. Gamble, A. Juliusson, T. Gärling, *Energy Policy* **2008**, *36*, 768–774.
[7] Y. Shao, M. F. El-Kady, J. Sun, Y. Li, Q. Zhang, M. Zhu, H. Wang, B. Dunn, R. B. Kaner, *Chem. Rev.* **2018**, *118*, 9233–9280.
[8] K. Sharma, A. Arora, S. K. Tripathi, *J. Energy Storage* **2019**, *21*, 801–825.
[9] P. Simon, Y. Gogotsi, B. Dunn, *Science* **2014**, *343*, 1210–1211.
[10] C. Largeot, C. Portet, J. Chmiola, P. Taberna, Y. Gogotsi, P. Simon, *J. Am. Chem. Soc.* **2008**, *130*, 2730–2731.
[11] R. Burt, G. Birkett, X. S. Zhao, *Phys. Chem. Chem. Phys.* **2014**, *16*, 6519–6538.
[12] C. Costentin, T. R. Porter, J.-M. Savéant, *ACS Appl. Mater. Interfaces* **2017**, *9*, 8649–8658.
[13] N. R. Chodankar, H. D. Pham, A. K. Nanjundan, J. F. S. Fernando, K. Jayaramulu, D. Golberg, Y. Han, D. P. Dubal, *Small* **2020**, *16*, 2002806.
[14] Q. Lu, J. G. Chen, J. Q. Xiao, *Angew. Chem. Int. Ed.* **2013**, *52*, 1882–1889.
[15] P. Bhojane, *J. Energy Storage* **2022**, *45*, 103654.
[16] Y. Song, T. Liu, X. Xu, D. Feng, Y. Li, X. Liu, *Adv. Funct. Mater.* **2015**, *25*, 4626–4632.
[17] X. Ji, P. S. Herle, Y. Rho, L. F. Nazar, *Chem. Mater.* **2007**, *19*, 374–383.
[18] A. Bhaskar, M. Deepa, T. Narasinga Rao, *ACS Appl. Mater. Interfaces* **2013**, *5*, 2555–2566.
[19] X. Hu, W. Zhang, X. Liu, Y. Mei, Y. Huang, *Chem. Soc. Rev.* **2015**, *44*, 2376–2404.
[20] J. Rajeswari, P. S. Kishore, B. Viswanathan, T. K. Varadarajan, *Electrochem. Commun.* **2009**, *11*, 572–575.
[21] F. Gao, L. Zhang, S. Huang, *Mater. Lett.* **2010**, *64*, 537–540.
[22] P. Han, W. Ma, S. Pang, Q. Kong, J. Yao, C. Bi, G. Cui, *J. Mater. Chem. A* **2013**, *1*, 5949–5954.
[23] X. Li, J. Shao, J. Li, L. Zhang, Q. Qu, H. Zheng, *J. Power Sources* **2013**, *237*, 80–83.
[24] K. M. Hercule, Q. Wei, A. M. Khan, Y. Zhao, X. Tian, L. Mai, *Nano Lett.* **2013**, *13*, 5685–5691.
[25] L. Mai, H. Li, Y. Zhao, L. Xu, X. Xu, Y. Luo, Z. Zhang, W. Ke, C. Niu, Q. Zhang, *Sci. Rep.* **2013**, *3*, 1718.
[26] P. Sharma, T. S. Bhatti, *Energy Convers. Manage.* **2010**, *51*, 2901–2912.
[27] L. Zheng, Y. Xu, D. Jin, Y. Xie, *J. Mater. Chem.* **2010**, *20*, 7135–7143.
[28] Y. Zhang, B. Lin, Y. Sun, P. Han, J. Wang, X. Ding, X. Zhang, H. Yang, *Electrochim. Acta* **2016**, *188*, 490–498.
[29] Z. Yu, L. Tetard, L. Zhai, J. Thomas, *Energy Environ. Sci.* **2015**, *8*, 702–730.
[30] C. Yuan, X. Zhang, L. Su, B. Gao, L. Shen, *J. Mater. Chem.* **2009**, *19*, 5772–5777.
[31] L. Mai, F. Yang, Y. Zhao, X. Xu, L. Xu, Y. Luo, *Nat. Commun.* **2011**, *2*, 381.
[32] D. Sarkar, G. G. Khan, A. K. Singh, K. Mandal, *J. Phys. Chem. C* **2013**, *117*, 15523–15531.
[33] X. Xia, J. Tu, Y. Zhang, Y. Mai, X. Wang, C. Gu, X. Zhao, *RSC Adv.* **2012**, *2*, 1835–1841.
[34] M. Nehra, N. Dilbaghi, G. Marrazza, A. Kaushik, R. Abolhassani, Y. K. Mishra, K. H. Kim, S. Kumar, *Nano Energy* **2020**, *76*, 104991.
[35] C. Shi, K. A. Owusu, X. Xu, T. Zhu, G. Zhang, W. Yang, L. Mai, *Small* **2019**, *15*, 1902348.
[36] J. W. Long, B. Dunn, D. R. Rolison, H. S. White, *Chem. Rev.* **2004**, *104*, 4463–4492.
[37] H. J. Fan, P. Werner, M. Zacharias, *Small* **2006**, *2*, 700–717.
[38] L. Mai, X. Tian, X. Xu, L. Chang, L. Xu, *Chem. Rev.* **2014**, *114*, 11828–11862.
[39] M. J. Kennedy, S. C. Bevan, *J. Less-Common Met.* **1974**, *36*, 23–30.
[40] Y. Zhou, C. W. Lee, S.-K. Kim, S. Yoon, *ECS Electrochem. Lett.* **2012**, *1*, A17.
[41] L. Q. Mai, B. Hu, W. Chen, Y. Y. Qi, C. S. Lao, R. S. Yang, Y. Dai, Z. L. Wang, *Adv. Mater.* **2007**, *19*, 3712–3716.
[42] B. Hu, L. Mai, W. Chen, F. Yang, *ACS Nano* **2009**, *3*, 478–482.
[43] E. Zhou, C. Wang, Q. Zhao, Z. Li, M. Shao, X. Deng, X. Liu, X. Xu, *Ceram. Int.* **2016**, *42*, 2198–2203.
[44] L. Zhang, H. Lin, L. Zhai, M. Nie, J. Zhou, S. Zhuo, *J. Mater. Res.* **2017**, *32*, 292–300.
[45] X. Yuan, X. Yan, C. Zhou, D. Wang, Y. Zhu, J. Wang, X. Tao, X. Cheng, *Ceram. Int.* **2020**, *46*, 19981–19989.
[46] D. Wu, Y. Yang, P. Zhu, X. Zheng, X. Chen, J. Shi, F. Song, X. Gao, X. Zhang, F. Ouyang, *J. Phys. Chem. C* **2018**, *122*, 1860–1866.
[47] P. Ou, Q. Zhou, J. Li, W. Chen, J. Huang, L. Yang, J. Liao, M. Sheng, *Mater. Res. Express* **2019**, *6*, 95044.
[48] J. Ni, Y. Zhao, L. Li, L. Mai, *Nano Energy* **2015**, *11*, 129–135.
[49] D. Zheng, H. Feng, X. Zhang, X. He, M. Yu, X. Lu, Y. Tong, *Chem. Commun.* **2017**, *53*, 3929–3932.
[50] J. Zhou, N. S. Xu, S. Z. Deng, J. Chen, J. C. She, Z. L. Wang, *Adv. Mater.* **2003**, *15*, 1835–1840.
[51] X. Lu, Z. Huang, Y. Tong, G. Li, *Chem. Sci.* **2016**, *7*, 510–517.
[52] X. Xiao, Z. Peng, C. Chen, C. Zhang, M. Beidaghi, Z. Yang, N. Wu, Y. Huang, L. Miao, Y. Gogotsi, *Nano Energy* **2014**, *9*, 355–363.
[53] R. Razaq, D. Sun, Y. Xin, Q. Li, T. Huang, Z. Zhang, Y. Huang, *Adv. Mater. Interfaces* **2019**, *6*, 1801636.
[54] S. Wang, B. Yang, H. Chen, E. Ruckenstein, *Energy Storage Mater.* **2019**, *16*, 619–624.
[55] V. Ramakrishnan, C. Alex, A. N. Nair, N. S. John, *Chem. Eur. J.* **2018**, *24*, 18003–18011.
[56] Y. W. Lee, M. C. Kim, Q. H. Nguyen, W. Ahn, J. E. Jung, K. W. Park, J. I. Sohn, *Ceram. Int.* **2019**, *45*, 2670–2675.
[57] J. Wang, J. Polleux, J. Lim, B. Dunn, *J. Phys. Chem. C* **2007**, *111*, 14925–14931.
[58] T. Brezesinski, J. Wang, S. H. Tolbert, B. Dunn, *Nat. Mater.* **2010**, *9*, 146–151.
[59] X. Yuan, X. Yan, C. Zhou, D. Wang, Y. Zhu, J. Wang, X. Tao, X. Cheng, *Ceram. Int.* **2020**, *46*, 19981–19989.
[60] H.-S. Kim, J. B. Cook, S. H. Tolbert, B. Dunn, *J. Electrochem. Soc.* **2015**, *162*, A5083–A5090.

Manuscript received: May 11, 2022
Revised manuscript received: June 19, 2022
Accepted manuscript online: July 1, 2022
Version of record online: July 18, 2022